IEEE Access
Multidisciplinary | Rapid Review | Open Access Journal

Received May 22, 2019, accepted June 10, 2019, date of publication June 14, 2019, date of current version July 1, 2019.

Digital Object Identifier 10.1109/ACCESS.2019.2923067

Speckle Noise Removal Convex Method Using Higher-Order Curvature Variation

BAOXIANG HUANG[1], (Member, IEEE), YUNPING MU[1], ZHENKUAN PAN[1], LI BAI[2], HUAN YANG[1], (Member, IEEE), AND JINMING DUAN[3]

[1]College of Computer Science and Technology, Qingdao University, Qingdao 266071, China
[2]School of Computer Science and Information Technology, The University of Nottingham, Nottingham NG8 1BB, U.K.
[3]School of Computer Science, The University of Birmingham, Birmingham B15 2TT, U.K.

Corresponding author: Huan Yang (cathy_huanyang@hotmail.com)

This work was supported in part by the National Natural Science Foundation of China under Grant 61602269, in part by the Natural Science Foundation of Shandong Province, China, under Grant ZR2017MD004, in part by the China Postdoctoral Science Foundation under Grant 2015M571993, and in part by the Young Teachers' Growth Plan of Shandong Province.

ABSTRACT In order to remove speckle noise while preserving image features, a novel variational model for image restoration based on total curvature is proposed in this paper. Due to the characteristics of nonlinear, non-convex, and non-smooth, the proposed variational model is transformed into an alternating optimization problem through introducing a series of auxiliary variables and using the alternating direction method of multipliers. In each loop of optimization, the Fast Fourier Transform is employed to solve the involved partial differential equations numerically, and the generalized soft thresholding formula is used to solve the involved algebra equations analytically. Moreover, the projection method is applied to fulfill some related inequality constraints simply for different sub-problems, thus the computational efficiency is improved totally. The numerous experiments on synthetic and real cases are implemented to demonstrate the advantages of the proposed model in image edge and corner preserving, and to indicate the high computation efficiency of the designed algorithm through comparison with other fast algorithms.

INDEX TERMS Speckle noise, curvature-dependent, alternating direction method of multipliers, discrete Fourier transform.

I. INTRODUCTION

Digital images are usually accompanied with speckle noise in many coherent imaging systems, such as laser images, ultrasound images, Synthetic Aperture Radar (SAR) images, microscope images, etc [1]. It degrades image quality and erects barriers to interpret valuable information of images. Consequently, in the area of image processing, speckle noise removal has been extensively studied [2]–[7].

Assuming that original image u is corrupted by speckle noise η, the restoration process aims to recover u from degrade image $f = u\eta$, and preserve image features including edges, point target, textures, and so on. To achieve this objective, a variety of speckle noise removal methods have been proposed. Some methods have been well-known, such as traditional filtering [8], wavelets approaches [9], principal component analysis-based approaches [10], and variational methods [11]. The variational method in image processing is to search numerical approximation to the lowest energy function of image [12], further the variational principle is the foundation of this method [13]. The focus of this study is to extend the variational method for speckle noise removal.

Speckle noise is non-Gaussian, signal and spatially independent [14]–[16]. Consequently, speckle noise removal is more complex and more challenging than additive noise removal. The speckle noise is described by different probability density function, includes Gamma, Poisson and Rayleigh distribution functions [17]. Over the past two decades, there are several variational approaches for addressing speckle noise removal problem. Variational model for speckle noise removal normally consists of regularized term and data fidelity term, and the regularized term is commonly designed as Total Variation (TV) [18]. A speckle noise removal model (RLO-model) was firstly advocated by Rudin et al with assumption of Gauss white noise [19]. For Gamma noise, a variational model (AA-model) via the maximum of

The associate editor coordinating the review of this manuscript and approving it for publication was Sudhakar Radhakrishnan.

TABLE 1. Speckle noise removal variational model based on TV framework.

Probability density	Data fidelity term	Model abbre	Author
Gauss distribution	$\frac{1}{2}\int_{\Omega}\left(\frac{f}{u}-1\right)^2 dx$	RLO	Rudin,Lions, Osher
Gamma distribution	$\int_{\Omega}\left(\frac{f}{u}+logu\right)dx$	AA	Auber, Aujol
Gamma distribution	$\int_{\Omega}\left(u+fe^{-u}\right)dx$	JY	Jin,Yang
Poisson	$\int_{\Omega}\left(u-flogu\right)dx$	SST	Setzer,Steidl, Tueber
Rayleigh	$\int_{\Omega}\left(\frac{1}{2}\left(\frac{f}{u}\right)^2+logu\right)dx$	DTDS	Denis,Tupin, Darbon, Sigelle
General	$\int_{\Omega}\left(a\frac{f}{u}+\frac{b}{2}\left(\frac{f}{u}\right)^2+c\log u\right)dx$	SO	Shi, Osher

a posteriori estimator was derived by Auber and Aujol [20]. Motivated by the effectiveness of the inverse scale space, Shi and Osher developed a strictly convex general model (SO-model) for speckle noise removal [21]. Involving non-convex and non-smooth [22] log-likelihood terms, Markov random field was extended to speckle noise removal, and the Bayesian type variational model (DTDS-model) was introduced by Denis et al. [23]. By applying I-divergence as similarity term, an energy functional (SST-model) was presented for degraded images with Poisson noise [24]. Applying exponential transformation $u \rightarrow e^u$ to AA model [3], globally convex model (JY-model) for speckle noise removal had been achieved [25]. In general, the TV framework for speckle noise removal can be summarized as Table 1.

Most speckle noise removal works are the transformation or combination of above mentioned data fidelity terms [7], [26], [27] and joint with additive noise removal [28]. TV regularization performs well in preserving edges, however, it suffers from staircase effect [29]. To attack this problem, higher order Partial Differential Equations (PDEs) were introduced [30]. Distinguished with TV regularization, the basis of these methods is minimizing the derivatives of the image [31]. The high order regularizations mainly contain bounded Hessian $\nabla^2 u$ regularization [32], Laplacian Δu regularization, total generalized variation [33], [34] and total curvature $\nabla \cdot \left(\frac{\nabla u}{|\nabla u|}\right)$ regularization [35], [36]. Due to the computational complexity and nonlinear of these higer order terms, little research has been done on higher-order variational model for speckle noise removal [37]. In combination with data fidelity terms in Table 1, this paper aims to propose a novel speckle noise removal variational model with mean total curvature regularization term.

As mentioned above, previous studies mostly focused on constructing speckle noise removal variational models. In order to solve the minimization problems related to Euler-Lagrange formulas of TV variational model, many fast algorithms have been proposed [38]–[43]. The algorithm for speckle noise removal numerical approximation mainly adopted the algorithm of classic TV model, such as fixed point method [44], semi-implicit iteration [45], dual method [39], [46], [47], Split Bregman algorithm [48], inverse scale space method [21], [49], multi-grid method [7] and so on. Higher order variational models will result in complicated high-order nonlinear PDEs which are difficult for discretization. Motivated by the Split Bregman scheme, combing with operator splitting, relaxation method and Augmented Lagrangian Method (ALM), a fast algorithm for Euler's elastica model was proposed by Tai et al [50]. In order to improve computational efficiency, the high-order model was transformed into several sub-problems by split Bregman scheme. Then the sub-problems could be calculated with analytical soft thresholding equation, fast Fourier transform (FFT), and projection formula [12]. The data fidelity term and curvature regularization of proposed speckle noise removal model are both not convex and nonlinear. Hence, efficient and stable numerical scheme to solve this problem is much desired. Inspired by the work from Tai [50] and Lu [12], this paper proposes an efficient and fast numerical algorithm to solve minimization problem related to high-order speckle noise removal variational model.

The objective of this work is to propose a novel higher order variational model for speckle noise removal. Combing with data fidelity term, the model adopts the total curvature as a regularization. Further, the proposed model is retransformed to an optimization problem with constraints by operator splitting and relaxation method. Besides, we adopt alternating direction method of multipliers (ADMM) to design a fast numerical approximation iterative scheme. Finally, the numerical experiments are implemented to illustrate that the proposed method can achieve highly restoration results.

The outline of this paper is as follows. Section 2 defines some notations for addressing the problem. In section 3, our proposed model is described in which the speckle noise removal problem is divided into some sub-problems by employing operator splitting idea. Alternating minimization iterative scheme and numerical approximation methods are detailed described in Section 4. To verify the superiority of the proposed method, extensive experiments are demonstrated in Section 5. Section 6 is the conclusion of the paper.

II. NOTATIONS

Before proceeding, let us briefly introduce some notations for convenience. Let $\Omega \rightarrow \Re^{M\times N}$ be a set of $M \times N$ points, and denote the two-dimensional grey scale image space $\Re$ with size of $M \times N$. The coordinates x and y are oriented along rows and columns, respectively. The first order forward differences

of u at point (i, j) can be written as follows.

$$\begin{aligned}
\partial_x{}^+ u_{i,j} &= \begin{cases} u_{i+1,j} - u_{i,j} & if\ 1 \le i < N \\ u_{1,j} - u_{N,j} & if\ i = N \end{cases} \\
\partial_x{}^- u_{i,j} &= \begin{cases} u_{i,j} - u_{i-1,j} & if\ 1 \le i < N \\ u_{1,j} - u_{N,j} & if\ i = 1 \end{cases} \\
\partial_y{}^+ u_{i,j} &= \begin{cases} u_{i,j+1} - u_{i,j} & if\ 1 \le j < M \\ u_{i,1} - u_{i,M} & if\ j = M \end{cases} \\
\partial_y{}^- u_{i,j} &= \begin{cases} u_{i,j} - u_{i,j-1} & if\ 1 \le j < M \\ u_{i,1} - u_{i,M} & if\ j = 1 \end{cases}
\end{aligned} \tag{1}$$

Boundary conditions of Euler-Lagrange equation are very crucial in numerical approximation. In order to apply FFT method, we utilize periodic boundary conditions, rather than Neumann boundary conditions used in SO-model. The gradient, Laplacian, gradient of divergence will be implemented for proposed model, which can be discretized as following formula.

$$\nabla u = \begin{bmatrix} \partial_x{}^+ u \\ \partial_y{}^+ u \end{bmatrix} \tag{2}$$

$$\nabla \cdot \nabla z = (\partial_x{}^- \partial_x{}^+ + \partial_y{}^- \partial_y{}^+) z \tag{3}$$

$$\nabla (\nabla \cdot \vec{n}) = \begin{bmatrix} \partial_x{}^- \partial_x{}^+ n_1 + \partial_x{}^- \partial_y{}^+ n_2 \\ \partial_y{}^- \partial_x{}^+ n_1 + \partial_y{}^- \partial_y{}^+ n_2 \end{bmatrix} \tag{4}$$

Referencing the method in [50], for $f_{ij} \in \Re^{M \times N}$, we introduce the shifting operators $\mathcal{S}_1{}^{\pm}$, $\mathcal{S}_2{}^{\pm}$, and identity operator $\mathcal{I}$ as follows.

$$\mathcal{S}_1{}^{\pm} f_{i,j} = f_{i \pm 1,j}, \quad \mathcal{S}_2{}^{\pm} f_{i,j} = f_{i,j \pm 1}, \ \mathcal{I} f_{i,j} = f_{i,j} \tag{5}$$

In frequency domain, the Discrete Fourier Transform (DFT) of shifting operator is the componentwise multiplication, which can be obtained by applying DFT. For discrete frequencies, $y_i = 1, 2, \cdots N$ and $y_j = 1, 2, \cdots M$, the $\mathcal{F}$ is obtained.

$$\mathcal{F}\mathcal{S}_1{}^{\pm} f_{y_i,y_j} = e^{\pm\sqrt{-1} z_i} \mathcal{F} f_{y_i,y_j}, \quad z_i = \frac{2\pi}{N} y_i \tag{6}$$

$$\mathcal{F}\mathcal{S}_2{}^{\pm} f_{y_i,y_j} = e^{\pm\sqrt{-1} z_j} \mathcal{F} f_{y_i,y_j}, \quad z_j = \frac{2\pi}{M} y_j \tag{7}$$

where $e^{\pm\sqrt{-1} z_i} = \cos z_i \pm \sqrt{-1} \sin z_i$ and $e^{\pm\sqrt{-1} z_i} = \cos z_j \pm \sqrt{-1} \sin z_j$. By upper transformation, high order Euler equation could be solved by the FFT to obtain algebraic equation, then use inverse DFT to obtain optimization variable. It is note that the variable result is the real part of a complex number, and we sign as $R(\cdot)$.

III. PROPOSED MODEL

A. A BRIEF REVIEW OF STRICTLY CONVEX SO-MODEL

By applying logarithm transform to $f = u\eta$, the multiplicative noise is converted to addictive noise, and we can achieve following equation.

$$\log f = \log u + \log \eta \tag{8}$$

Based on noisy observation $\log f$, $TV(\log u)$ is substitute for the regularization $TV(u)$ and let $w = \log u$, a general TV formulation for speckle noise can be gained.

$$\min E(u) = \int_\Omega |\nabla u| + \lambda \int_\Omega \left(a\frac{f}{u} + \frac{b}{2}\left(\frac{f}{u}\right)^2 + c \log u \right) \tag{9}$$

where a, b, c are nonnegative constants. Gradient descent method can be used to solve Eq.(9), and the following Euler-Lagrange equation can be obtained.

$$u_t = \nabla \cdot \frac{\nabla u}{|\nabla u|} + \lambda \left(a\frac{f}{u^2} + b\frac{f^2}{u^3} - c\frac{1}{u} \right) \tag{10}$$

Due to the mapping $w \to e^w$ is strictly monotonous increasing, applying a partial transformation which is replace $u = e^w$ by w, the fidelity term was then rendered convex. The TV based minimization can be obtained.

$$\min E(w) = \int_\Omega |\nabla w| + \lambda \int_\Omega \left(a f e^{-w} + \frac{b}{2} f^2 e^{-2w} + cw \right) \tag{11}$$

B. A NEW CURVATURE BASED CONVEX MODEL (CSN)

Enlightened by SO-model, we propose the following higher order mean curvature regularized model.

$$\begin{aligned}
\min E(u) = &\int_\Omega \left| \nabla \cdot \frac{\nabla u}{|\nabla u|} \right| dx \\
&+ \alpha \int_\Omega \left(a\frac{f}{u} + \frac{b}{2}\left(\frac{f}{u}\right)^2 + c \ln u \right) dx
\end{aligned} \tag{12}$$

To overcome the lack of global convexity, we introduce variable $u = e^z$. While the mean curvature regularization term is left unaltered, the problem Eq.(12) is transformed into the following minimization functional with a convex data fidelity term.

$$\begin{aligned}
\min E(z) = &\int_\Omega \left| \nabla \cdot \frac{\nabla z}{|\nabla z|} \right| dx \\
&+ \alpha \int_\Omega \left(a f e^{-z} + \frac{b}{2} f^2 e^{-2z} + cz \right) dx
\end{aligned} \tag{13}$$

Although the curvature regularization term has high effectiveness in removing staircase effect, the minimization of the corresponding functional Eq.(13) is a very challenging problem. The Euler-Lagrange equations of the regularization are the fourth order nonlinear PDEs, hence, it is very difficult to discretize for numerical approximation. Here, we first employ splitting operators $w, \vec{p}, \vec{n}$ and q to simplify curvature regularization as following constrained energy functional.

$$\begin{aligned}
&\min E(z) = \int_\Omega |q| dx dy + \alpha \int_\Omega \left(a f e^{-w} + \frac{b}{2} f^2 e^{-2w} + cw \right) dx dy \\
&s.t.\ w = z, \quad \vec{p} = \nabla z, \ \vec{n} = \frac{\vec{p}}{|\vec{p}|}, \ q = \nabla \cdot (\vec{n})
\end{aligned} \tag{14}$$

Then, according to well-known Holder inequality, we transform $\vec{n} = \vec{p}/|\vec{p}|$ into $|\vec{n}| \le 1$ and $|p| = \vec{n} \cdot \vec{p}$ equivalent

constraints. Finally, the constraint $\vec{m} = \vec{n}$ is designed, consequently, $\vec{n} = \vec{p}/|\vec{p}|$ can be converted into $|\vec{m}| \leq 1$ and $|p| = \vec{m} \cdot \vec{p}$. In fact, variable $\vec{m}$ with $|\vec{m}| \leq 1$ is relaxation. Hence, the minimization of the functional in Eq.(14) is equivalent to the following minimization problem with constraints.

$$\begin{aligned} \min E(z) &= \int_\Omega |q| dxdy \\ &+ \alpha \int_\Omega \left(af e^{-w} + \frac{b}{2} f^2 e^{-2w} + cw \right) dxdy \\ s.t.\ w &= z, \quad |p| = \vec{m} \cdot \vec{p},\ \vec{p} = \nabla u,\ q = \nabla \cdot (\vec{n}), \\ \vec{n} &= \vec{m}, \quad |\vec{m}| \leq 1 \end{aligned} \tag{15}$$

Though these changes may seem trivial, now ALM can be used to solve upper problem Eq.(15). We use L^2 penalization for constraints $w = z$, $\vec{p} = \nabla u$, $q = \nabla \cdot (\vec{n})$ and $\vec{n} = \vec{m}$. For $|\vec{m}| \leq 1$, we can deduce that $|p| - \vec{m} \cdot \vec{p} \geq 0 \, in \, \Omega$, so we use L^1 penalization for constraint $|p| = \vec{m} \cdot \vec{p}$. Thus, the proposed constrained optimization problem Eq.(15) can be efficiently solved with the following augmented Lagrangian functional.

$$\begin{aligned} &\left(z, w, \vec{p}, q, \vec{n}, \vec{m}\right) \\ &= \underset{z,w,\vec{p},q,\vec{n},\vec{m}}{\arg\min} \left\{ \begin{aligned} &\int_\Omega |q| dxdy \\ &+\alpha \int_\Omega \left(af e^{-w} + \frac{b}{2} f^2 e^{-2w} + cw \right) dxdy \\ &+\frac{\beta_1}{2} \int_\Omega (z-w)^2 dxdy \\ &+ \int_\Omega \lambda_1 (z-w) dxdy \\ &+\beta_2 \int_\Omega (|\vec{p}| - \vec{m} \cdot \vec{p}) dxdy \\ &+ \int_\Omega \lambda_2 (|\vec{p}| - \vec{m} \cdot \vec{p}) dxdy \\ &+\frac{\beta_3}{2} \int_\Omega (\vec{p} - \nabla u)^2 dxdy \\ &+ \int_\Omega \vec{\lambda}_3 \cdot (\vec{p} - \nabla u) dxdy \\ &+\frac{\beta_4}{2} \int_\Omega (q - \nabla \cdot \vec{n})^2 dxdy \\ &+ \int_\Omega \lambda_4 (q - \nabla \cdot \vec{n}) dxdy \\ &+\frac{\beta_5}{2} \int_\Omega |\vec{n} - \vec{m}|^2 dxdy \\ &+ \int_\Omega \vec{\lambda}_5 \cdot (\vec{n} - \vec{m}) dxdy \end{aligned} \right. \end{aligned} \tag{16}$$

where β_1, β_2, β_3, β_4, β_5 are positive penalty parameters, λ_1, λ_2, $\vec{\lambda}_3$, λ_4, $\vec{\lambda}_5$ are Lagrange multipliers, which can be updated according to the rules. The primal variable u denotes the denoising image, z is the log of u, dual variable w is the log of u, $\vec{p}$ is a vector function regarding gradient of u, q is a scalar valued function regarding divergence of vector $\vec{n}$, $\vec{n}$ is also a vector function regarding the unit vector of the level curves of u, $\vec{m}$ is a vector valued function introduced to relax variable $\vec{n}$. In next section, we will show the details of implementation for Eq.(16).

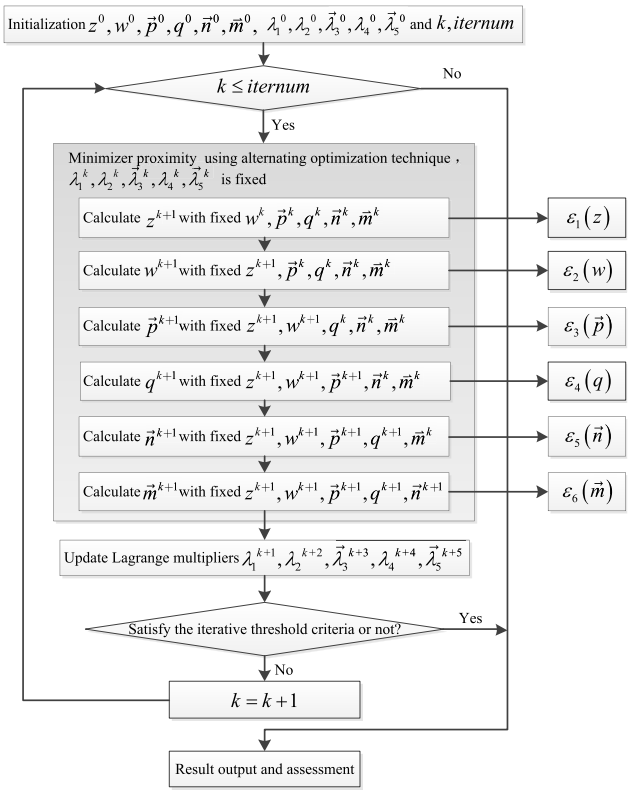

FIGURE 1. Alternating minimization iterative algorithm to solve the problem.

IV. FAST NUMERICAL METHODS

The problem Eq.(16) is a multivariable energy functional, we employ the ADMM to design an iterative scheme. Furthermore, compound numerical approximation method is also implemented in this section, including gradient descend, soft thresholding formula, FFT and projection method.

A. ALTERNATING MINIMIZATION ITERATIVE SCHEME

In convex optimization, the saddle point of the augmented Lagrangian functional will lead to a minimize solution. The ADMM is the integration scheme of the many classical optimization idea, updates dual variable with partial, and the convergence of ADMM is always guaranteed [50]. With ADMM, an iterative scheme can be employed to search optimal solution of Eq.(16) guaranteeing the first order condition. The proposed iterative scheme is presented in Figure 1.

The variables $w^0, \vec{p}^0, q^0, \vec{n}^0, \vec{m}^0$ and Lagrange multipliers $\lambda_1{}^0, \lambda_2{}^0, \vec{\lambda}_3^0, \lambda_4{}^0, \vec{\lambda}_5^0$ are simply initialized to zero. Avoiding $\log(f)$ is too small or zero to difficult computation, z^0 is initialized to $3\log(f+1)$. For iterative number $k \geq 1$, with the fixed Lagrange multipliers $\lambda_1{}^k, \lambda_2{}^k, \vec{\lambda}_3^k, \lambda_4{}^k, \vec{\lambda}_5^k$, alternating minimization method is adopted to calculate (z^{k+1}, w^{k+1}, $\vec{p}^{k+1}$, q^{k+1}, $\vec{n}^{k+1}$, $\vec{m}^{k+1}$) of the Lagrange functional. So,

problem (16) is transformed into the following sub-problems.

$$\begin{aligned}\varepsilon_1(z) &= \frac{\beta_1}{2}\int_\Omega \left(z-w^k\right)^2 dxdy + \int_\Omega {\lambda_1}^k\left(z-w^k\right)dxdy \\ &+ \frac{\beta_3}{2}\int_\Omega \left(\vec{p}^k-\nabla z\right)^2 dxdy \\ &+ \int_\Omega \vec{\lambda}_3^k\left(\vec{p}^k-\nabla z\right)dxdy \end{aligned} \tag{17}$$

$$\begin{aligned}\varepsilon_2(w) &= \alpha\int_\Omega \left(af e^{-w}+\frac{b}{2}f^2e^{-2w}+cw\right)dxdy \\ &+ \frac{\beta_1}{2}\int_\Omega \left(z^{k+1}-w\right)^2 dxdy \\ &+ \int_\Omega {\lambda_1}^k\left(z^{k+1}-w\right)dxdy \end{aligned} \tag{18}$$

$$\begin{aligned}\varepsilon_3(\vec{p}) &= \beta_2\int_\Omega \left(|\vec{p}|-\vec{m}^k\cdot\vec{p}\right)dxdy \\ &+ \int_\Omega \lambda_2^k\left(|\vec{p}|-\vec{m}^k\cdot\vec{p}\right)dxdy \\ &+ \frac{\beta_3}{2}\int_\Omega \left(\vec{p}-\nabla z^{k+1}\right)^2 dxdy \\ &+ \int_\Omega \vec{\lambda}_3^k\left(\vec{p}-\nabla z^{k+1}\right)dxdy \end{aligned} \tag{19}$$

$$\begin{aligned}\varepsilon_4(q) &= \int_\Omega |q|dxdy + \frac{\beta_4}{2}\int_\Omega \left(q-\nabla\cdot\vec{n}^k\right)^2 dxdy \\ &+ \int_\Omega \lambda_4^k\left(q-\nabla\cdot\vec{n}^k\right)dxdy \end{aligned} \tag{20}$$

$$\begin{aligned}\varepsilon_5(\vec{n}) &= \frac{\beta_4}{2}\int_\Omega \left(q^{k+1}-\nabla\cdot\vec{n}\right)^2 dxdy \\ &+ \int_\Omega \lambda_4^k\left(q^{k+1}-\nabla\cdot\vec{n}\right)dxdy \\ &+ \frac{\beta_5}{2}\int_\Omega \left|\vec{n}-\vec{m}^k\right|^2 dxdy + \int_\Omega \vec{\lambda}_5^k\cdot\left(\vec{n}-\vec{m}^k\right)dxdy \end{aligned} \tag{21}$$

$$\begin{aligned}\varepsilon_6(\vec{m}) &= \beta_2\int_\Omega (|\vec{p}|-\vec{m}\cdot\vec{p})dxdy + \int_\Omega {\lambda_2}^k(|\vec{p}|-\vec{m}\cdot\vec{p})dxdy \\ &+ \frac{\beta_5}{2}\int_\Omega |\vec{n}-\vec{m}|^2 dxdy + \int_\Omega \vec{\lambda}_5^k\cdot(\vec{n}-\vec{m})dxdy \end{aligned} \tag{22}$$

The corresponding Euler equation of Eq.(17)-(22) can be obtained for next step numerical approximation. The minimization of Euler equation of $\varepsilon_2(w)$ can be done by gradient descend, $\varepsilon_3(\vec{p})$ and $\varepsilon_4(q)$ can be solved by soft thresholding formula, $\varepsilon_6(\vec{m})$ can be simply obtained by projection method. While the Euler equation of $\varepsilon_1(z)$ and $\varepsilon_5(\vec{n})$ are nonlinear equation over the whole image domain Ω, the FFT can be used to solve these two sub-problems.

After each iteration, update Lagrange multipliers ${\lambda_1}^{k+1}$, ${\lambda_2}^{k+1}$, $\vec{\lambda}_3^{k+1}$, ${\lambda_4}^{k+1}$, $\vec{\lambda}_5^{k+1}$ based on

$$\begin{aligned}{\lambda_1}^{k+1} &= {\lambda_1}^k + \beta_1\left(z^{k+1}-w^{k+1}\right), \\ {\lambda_2}^{k+1} &= {\lambda_2}^k + \beta_2\left(\left|\vec{p}^{k+1}\right|-\vec{m}^{k+1}\cdot\vec{p}^{k+1}\right), \\ \vec{\lambda}_3^{k+1} &= \vec{\lambda}_3^k + \beta_3\left(\vec{p}^{k+1}-\nabla u^{k+1}\right), \end{aligned}$$

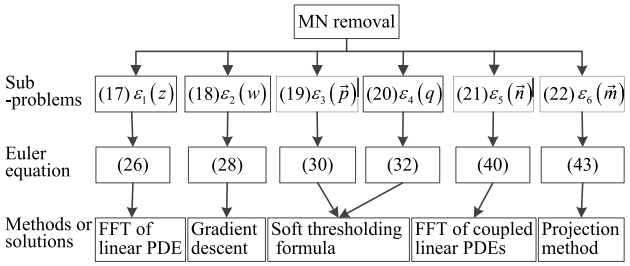

FIGURE 2. Implementation methods or solutions for problems.

$$\begin{aligned}{\lambda_4}^{k+1} &= {\lambda_4}^k + \beta_4\left(q^{k+1}-\nabla\cdot\vec{n}^{k+1}\right), \\ \vec{\lambda}_5^{k+1} &= \vec{\lambda}_5^k + \beta_5\left(\vec{n}^{k+1}-\vec{m}^{k+1}\right). \end{aligned} \tag{23}$$

B. NUMERICAL APPROXIMATION

For clarity, the implementation methods or solutions to solve energy functional minimization in Eq.(17)-(22) can be shown in Figure 2. All speckle noise removal sub-problems can be solved with high computational efficiency.

1) MINIMIZATION OF $\varepsilon_1(z)$ In (17)

With fixed w^k, $\vec{p}^k$ and ${\lambda_1}^k$, $\vec{\lambda}_3^k$, we can obtained the following Euler Lagrange equation of Eq.(17) with respect to z.

$$\begin{cases}\beta_1\left(z-w^k\right)+{\lambda_1}^k+\nabla\cdot\left(\beta_3\left(\vec{p}^k-\nabla z\right)+\vec{\lambda}_3^k\right)=0 & in\ \Omega \\ \beta_3\left(\vec{p}^k-\nabla z\right)+\vec{\lambda}_3^k=0 & on\ \partial\Omega\end{cases} \tag{24}$$

The expansion formula of Eq.(24) yields a linear equation.

$$\beta_5 z-\beta_2\nabla\cdot\nabla z=g,\quad g=\beta_5 w-{\lambda_5}^k-\nabla\cdot\beta_2\vec{p}-\nabla\cdot\vec{\lambda}_2^k. \tag{25}$$

Using the notations in Section 2, Eq.(25) can be efficiently solved by FFT. And Eq.(25) can be written as $\beta_1 z-\beta_3(\partial_x{}^-\partial_x{}^+ + \partial_y{}^-\partial_y{}^+)z = g$, $g = \beta_1 e^w - {\lambda_1}^k - \beta_3\left(\partial_x{}^- p_1{}^k + \partial_y{}^- p_2{}^k\right) - \left(\partial_x{}^-\lambda_{31}{}^k + \partial_y{}^-\lambda_{32}{}^k\right)$. The identity operator and shifting operators can be utilized to discretization. By applying the DFT $\mathcal{F}$ we obtain an algebraic equation $\underbrace{\left(\beta_1-2\beta_3\left(\cos z_i+\cos z_j-2\right)\right)}_{dz}\mathcal{F}z(i,j) = \mathcal{F}(g(i,j))$. Due to $dz = \left(\beta_1-2\beta_3\left(\cos z_i+\cos z_j-2\right)\right) > 0$, the discrete inverse Fourier transform $\mathcal{F}$ can be used to update z^{k+1}, then the final solution can be achieved.

$$z = R\left(\mathcal{F}^{-1}\left(\frac{\mathcal{F}(g)}{dz}\right)\right) \tag{26}$$

2) MINIMIZATION OF $\varepsilon_2(w)$ IN (18)

The Euler Lagrange equation of Eq.(18) with respect to w can be obtained with fixed z^{k+1} and ${\lambda_1}^k$.

$$\alpha\left(af e^{-w}+bf^2e^{-2w}-c\right)+\beta_1\left(z^{k+1}-w\right)+{\lambda_1}^k=0 \tag{27}$$

Here, we especially employ the value w^k of upper step to improve the computation speed. Then w^{k+1} can be simply calculated by gradient descend method, ∇t is time step for gradient descend.

$$w_{i,j}^{k+1} = w_{i,j}^k + \begin{pmatrix} \alpha\left(af_{i,j}e^{-w_{i,j}^k} + bf_{i,j}^2 e^{-2w_{i,j}^k} - c\right) \\ +\beta_1\left(z_{i,j}^{k+1} - w_{i,j}^k\right) + {\lambda_1}_{i,j}{}^k \end{pmatrix} \nabla t \tag{28}$$

3) MINIMIZATION OF $\varepsilon_3(\vec{p})$ IN (19)

Fixing variables z^{k+1}, $\vec{m}^k$ and ${\lambda_2}^k$, $\vec{\lambda}_3^k$, the Euler equation related to $\vec{p}$ can be achieved.

$$\beta_2 \frac{\vec{p}}{\left|\vec{p}\right|} - \beta_2 \cdot \vec{m}^k + {\lambda_2}^k \cdot \frac{\vec{p}}{\left|\vec{p}\right|} - {\lambda_2}^k \cdot \vec{m}^k + \beta_3\left(\vec{p} - \nabla z^{k+1}\right) + \vec{\lambda}_3^k = 0 \tag{29}$$

Eq.(29) can be easily solved by the analytical soft thresholding equation.

$$\vec{p}^{k+1} = \max\left(\left|\vec{t}_p\right| - \frac{\left(\beta_2 + {\lambda_2}^k\right)}{\beta_3}, 0\right)\frac{\vec{t}_p}{\left|\vec{t}_p\right|}, \quad 0\frac{\vec{0}}{\left|\vec{0}\right|} = 0$$
$$\vec{t}_p = \nabla z^{k+1} - \frac{\vec{\lambda}_3^k - \beta_2 \cdot \vec{m}^k - {\lambda_2}^k \cdot \vec{m}^k}{\beta_3} \tag{30}$$

4) MINIMIZATION OF $\varepsilon_4(q)$ IN (20)

The Euler Lagrange equation with respect to q can be obtained as follows.

$$\frac{q}{|q|} + \beta_4\left(q - \nabla \cdot \vec{n}^k\right) + {\lambda_4}^k = 0 \tag{31}$$

Arise from the minimization of energy functional Eq.(20) with fixed $\vec{n}^k$ and ${\lambda_4}^k$. We also employ the soft thresholding equations to solve this sub-problem.

$$q^{k+1} = \max\left(\left|\nabla \cdot \vec{n}^k - \frac{{\lambda_4}^k}{\beta_4}\right| - \frac{1}{\beta_4}, 0\right)\frac{\nabla \cdot \vec{n}^k - \frac{{\lambda_4}^k}{\beta_4}}{\left|\nabla \cdot \vec{n}^k - \frac{{\lambda_4}^k}{\beta_4}\right|}$$
$$0\frac{0}{|0|} = 0 \tag{32}$$

5) MINIMIZATION OF $\varepsilon_5(\vec{n})$ IN (21)

The Euler Lagrange equation of Eq.(21) for $\vec{n}$ with fixed q^{k+1}, $\vec{m}^k$, ${\lambda_4}^k$ and $\vec{\lambda}_5^k$ is given as follows formula.

$$\begin{cases} \beta_4\nabla\left(q^{k+1} - \nabla\cdot\vec{n}\right) + \nabla{\lambda_4}^k + \beta_5\left(\vec{n} - \vec{m}^k\right) + \vec{\lambda}_5^k = 0 & in\ \Omega \\ \left(\beta_4\left(q^{k+1} - \nabla\cdot\vec{n}\right) + \vec{\lambda}_4^k\right)\cdot\vec{n} = 0 & on\ \partial\Omega \end{cases} \tag{33}$$

Eq.(33) can be transformed into the following equation.

$$\beta_4\nabla\left(\nabla\cdot\vec{n}\right) - \beta_5\vec{n} = \underbrace{\beta_4\nabla q^{k+1} + \nabla{\lambda_4}^k + \vec{\lambda}_5^k - \beta_5\vec{m}^k}_{\vec{g}} \tag{34}$$

Here, $\vec{n}$ is a vector $\begin{bmatrix} n_1 \\ n_2 \end{bmatrix}$, hence, Eq.(34) is the coupled linear equation and can be solved by FFT efficiently.

We introduce vector variable $\vec{g} = \begin{bmatrix} g_1 \\ g_2 \end{bmatrix} = \beta_4\nabla q^{k+1} + \nabla{\lambda_4}^k + \vec{\lambda}_5^k - \beta_5\vec{m}^k$. Using shifting operators and identity operator, $\nabla\left(\nabla\cdot\vec{n}\right)$ can be given as follows.

$$\begin{aligned} &\nabla\left(\nabla\cdot\vec{n}\right) \\ &= \begin{bmatrix} {\partial_x}^-{\partial_x}^+ n_1 + {\partial_x}^-{\partial_y}^+ n_2 \\ {\partial_y}^-{\partial_x}^+ n_1 + {\partial_y}^-{\partial_y}^+ n_2 \end{bmatrix} \\ &= \begin{bmatrix} \left(\mathcal{I} - {\mathcal{S}_1}^-\right)\left({\mathcal{S}_1}^+ - \mathcal{I}\right)n_1 + \left(\mathcal{I} - {\mathcal{S}_1}^-\right)\left({\mathcal{S}_2}^+ - \mathcal{I}\right)n_2 \\ \left(\mathcal{I} - {\mathcal{S}_2}^-\right)\left({\mathcal{S}_1}^+ - \mathcal{I}\right)n_1 + \left(\mathcal{I} - {\mathcal{S}_2}^-\right)\left({\mathcal{S}_2}^+ - \mathcal{I}\right)n_2 \end{bmatrix} \end{aligned} \tag{35}$$

In order to simply the expression, we sign ${\mathcal{S}_1}^+ + {\mathcal{S}_1}^- - 2\mathcal{I}$ as $\mathcal{S}_{11}$, ${\mathcal{S}_2}^+ + {\mathcal{S}_1}^- - {\mathcal{S}_1}^-{\mathcal{S}_2}^+ - \mathcal{I}$ as $\mathcal{S}_{12}$, ${\mathcal{S}_1}^+ + {\mathcal{S}_2}^- - {\mathcal{S}_1}^+{\mathcal{S}_2}^- - \mathcal{I}$ as $\mathcal{S}_{21}$, and ${\mathcal{S}_2}^+ + {\mathcal{S}_2}^- - 2\mathcal{I}$ as $\mathcal{S}_{22}$. Then the left part of Eq.(34) $\beta_3\nabla\left(\nabla\cdot\vec{n}\right) - \beta_4\vec{n}$ is transformed as follows.

$$\beta_4\nabla\left(\nabla\cdot\vec{n}\right) - \beta_5\vec{n} = \begin{bmatrix} \beta_4\mathcal{S}_{11} - \beta_5 & \beta_4\mathcal{S}_{12} \\ \beta_4\mathcal{S}_{21} & \beta_4\mathcal{S}_{22} - \beta_5 \end{bmatrix}\begin{bmatrix} n_1 \\ n_2 \end{bmatrix} \tag{36}$$

Consequently, the Eq.(34) can be rewritten as follows.

$$\begin{bmatrix} \beta_4\mathcal{S}_{11} - \beta_5 & \beta_4\mathcal{S}_{12} \\ \beta_4\mathcal{S}_{21} & \beta_4\mathcal{S}_{22} - \beta_5 \end{bmatrix}\begin{bmatrix} n_1 \\ n_2 \end{bmatrix} = \begin{bmatrix} g_1 \\ g_2 \end{bmatrix} \tag{37}$$

Based on the discrete frequencies, applying the DFT to Eq.(37), the following linear equations can be obtained.

$$\begin{bmatrix} \underbrace{\mathcal{F}\left(\beta_4\mathcal{S}_{11} - \beta_5\right)}_{a_{11}} & \underbrace{\mathcal{F}\left(\beta_4\mathcal{S}_{12}\right)}_{a_{12}} \\ \underbrace{\mathcal{F}\left(\beta_4\mathcal{S}_{21}\right)}_{a_{21}} & \underbrace{\mathcal{F}\left(\beta_4\mathcal{S}_{22} - \beta_5\right)}_{a_{22}} \end{bmatrix}\begin{bmatrix} \mathcal{F}n_1 \\ \mathcal{F}n_2 \end{bmatrix} = \begin{bmatrix} \mathcal{F}g_1 \\ \mathcal{F}g_2 \end{bmatrix} \tag{38}$$

where the coefficients are:

$$\begin{aligned} a_{11} &= 2\beta_4\left(\cos z_i - 1\right) - \beta_5 \\ a_{12} &= \beta_4\left(\cos z_i - \sqrt{-1}\sin z_i - 1\right)\left(1 - \cos z_j - \sqrt{-1}\sin z_j\right) \\ a_{22} &= 2\beta_4\left(\cos z_j - 1\right) - \beta_5 \\ a_{21} &= \beta_4\left(\cos z_i + \sqrt{-1}\sin z_i - 1\right)\left(1 - \cos z_j + \sqrt{-1}\sin z_j\right) \end{aligned} \tag{39}$$

The coefficient matrix is $M \times N$ number of 2×2 systems. Just ensure parameter $\beta_4\beta_5 > 0$, the determinant $D = \beta_5 - 2\beta_4\beta_5\left(\cos z_i + \cos z_j - 2\right)$ is invariably positive. Consequently, the inverse DFT can be employed to obtain $\vec{n}$.

$$\begin{bmatrix} n_1 \\ n_2 \end{bmatrix} = \begin{bmatrix} R\left(\mathcal{F}^{-1}\left(\frac{a_{22}\mathcal{F}g_1 - a_{12}\mathcal{F}g_2}{D}\right)\right) \\ R\left(\mathcal{F}^{-1}\left(\frac{a_{11}\mathcal{F}g_2 - a_{21}\mathcal{F}g_1}{D}\right)\right) \end{bmatrix} \tag{40}$$

6) MINIMIZATION OF $\varepsilon_6(\vec{m})$ IN (22)

Variable $\vec{m}$ can be obtained from the following closed form with fixed $\vec{n}^{k+1}$, $\vec{p}^{k+1}$, ${\lambda_2}^k$ and $\vec{\lambda}_5^k$.

$$-\beta_2\vec{p}^{k+1} - {\lambda_2}^k\vec{p}^{k+1} + \beta_5\left(\vec{n}^{k+1} - \vec{m}\right)(-1) - \vec{\lambda}_5^k = 0 \tag{41}$$

It is note that constraint $|\vec{m}| \leq 1$ is of great importance to avoid unboundedness of $\vec{m}$ when $\vec{p} = 0$, furthermore, it can be treated as relaxation. Hence, the following projection formulation can be imposed on $\vec{m}$.

$$-\beta_2\vec{p}^{k+1} - {\lambda_2}^k\vec{p}^{k+1} + \beta_5\left(\vec{n}^{k+1} - \vec{m}\right)(-1) - \vec{\lambda}_5^k = 0 \tag{42}$$

$$\vec{m} = \begin{cases} \dfrac{\beta_2\vec{p}^{k+1} + {\lambda_2}^k\vec{p}^{k+1} + \vec{\lambda}_5^k}{\beta_5} + \vec{n}^{k+1} & |\vec{m}| \leq 1 \\ \dfrac{\frac{\beta_2\vec{p}^{k+1} + {\lambda_2}^k\vec{p}^{k+1} + \vec{\lambda}_5^k}{\beta_5} + \vec{n}^{k+1}}{\left|\frac{\beta_2\vec{p}^{k+1} + {\lambda_2}^k\vec{p}^{k+1} + \vec{\lambda}_5^k}{\beta_5} + \vec{n}^{k+1}\right|} & |\vec{m}| > 1 \end{cases} \tag{43}$$

C. ITERATIVE ALGORITHM

Now, all support functionals of problem Eq.(16) are computed for convex optimization. In other words, the stable and efficient minimization algorithm can be used to remove speckle noise. The alternating minimization iterative algorithm can be read as follows.

Algorithm 1 Alternating Minimization Iterative Algorithm

01: *function* *SNRemoval*(f)
02: Initialization: Set $z = 3\log(f+1)$, $w = z$, $\left(\vec{p}, q, \vec{n}, \vec{m}; \lambda_1, \lambda_2, \vec{\lambda}_3, \lambda_4, \vec{\lambda}_5\right) = 0$
$(\beta_1, \beta_2, \beta_3, \beta_4, \beta_5, \Delta t, iteration) > 0$, the value of a, b, c depends on the noise distribution function
03: Compute coefficient $a_{11}, a_{12}, a_{21}, a_{22}$ and determinant dz, D
04: repeat
05: Compute z according to Eq.(26)
06: Compute w according to Eq.(28)
07: Compute $\vec{p}$ according to Eq.(30)
08: Compute q according to Eq.(32)
09: Compute $\vec{n}$ according to Eq.(40)
10: Compute $\vec{m}$ according to Eq.(43)
11: Update Lagrangian multiplier $\lambda_1, \lambda_2, \vec{\lambda}_3, \lambda_4, \vec{\lambda}_5$ according to Eq.(23)
12: until convergence of u
13: return $u = e^{z/3} - 1$
14: end function

V. EXPERIMENTAL RESULTS

In this section, the performance of the proposed speckle noise removal method was evaluated based on images corrupted by synthetic multiplicative noise, real noisy SAR and real noisy biomedical images. Meanwhile, the results were compared with TV based AA, SST, DTDS, SO models and filter based Lee method. The detailed information of experiments is shown in Table 2.

TABLE 2. Detailed information of numerical experiments.

Experiment type	Serial number	Degraded image		Compared method
		Original images	Noise type	
Synthetic speckle noise	E01	Mixedgrid image	Gamma	AA model
	E02	Lena	Poisson	SST model
	E03	Boat	Rayleigh	DTDS model
	E04	68 Berkeley test images	Gamma/ Poisson/ Rayleigh	AA model SST model DTDS model Lee filter
Real SAR images	E05-1	SAR-1 image		AA model
	E05-2	SAR-2 image		
	E05-3	SAR-3 image		
Real biomedical images	E06-1	Biom-1 image		SO model
	E06-2	Biom-2 image		
	E06-3	Biom-3 image		

SO model is the comprehensive of AA and DTDS model, if $a = 1$, $b = 0$ and $c = 1$, SO model reduces to AA model, and when $a = 0$, $b = 1$ and $c = 1$, SO model reduces to DTDS model. The solution of SO and SST model was obtained by using Split-Bregman method. All experiments were performed using Matlab 2016b on a Windows 10 platform with an Intel Core i3-2120 CPU at 3.30GHz and 4GB memory.

Before we show our numerical results, we give some remarks on choosing tuning parameters. There are four parameters coming from the total curvature regularization and data fidelity term: the parameter α depends on how close we want u to be f. We tune α according to the amount of noise in an image: the noisier f is, the smaller the value is determined for α. Parameters a, b and c are determined by noise probability density function. For convex numerical algorithm, parameters $\beta_1, \beta_2, \beta_3, \beta_4, \beta_5$ are associated with Lagrange multipliers. In which, parameters $\beta_1, \beta_2, \beta_5$ mainly control the closeness between z and w, $|\vec{p}|$ and $\vec{m}\cdot\vec{p}$, $\vec{n}$ and $\vec{m}$, respectively, the parameters β_3, β_4 control the amount of diffusion of u, the larger β_3, β_4 are, the more diffusion u has, and the ratio between β_3 and β_4 has to do with the main factor of diffusion: larger β_4 encourages the total curvature diffusion. While using these as guideline, and to reduce the number of parameters to tune, we set $\beta_1, \beta_2, \beta_5 = 1$, $\frac{\beta_4}{\beta_3} = 10$ in numerical experiments, therefore, we just need to tune the parameter β_4. Consequently, the number of parameters associated with our algorithm is not of too much concern. In order to implement unified assessment, the stopping criteria of iteration for AA, SST, DTDS, SO and proposed model was defined as following formula.

$$\frac{E^k - E^{k-1}}{E^k} \leq threshold \tag{44}$$

E^k is the energy value of current step of iteration, and E^{k-1} is the energy value of upper step of iteration. The value of *threshold* for following experiments is 10^{-3}.

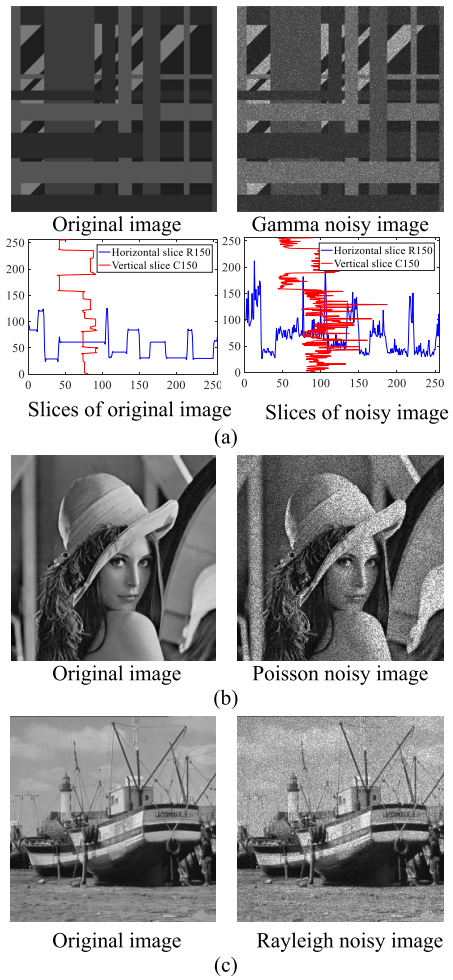

FIGURE 3. The problems for MN removal. (a) E01 experiment: Noise free and gamma noisy mixedgrid image, Horizontal and vertical slices for edge preservation analysis; (b) E02 experiment: Original and poisson noisy Lena image; (c) E03 experiment: Original and rayleigh noisy boat image.

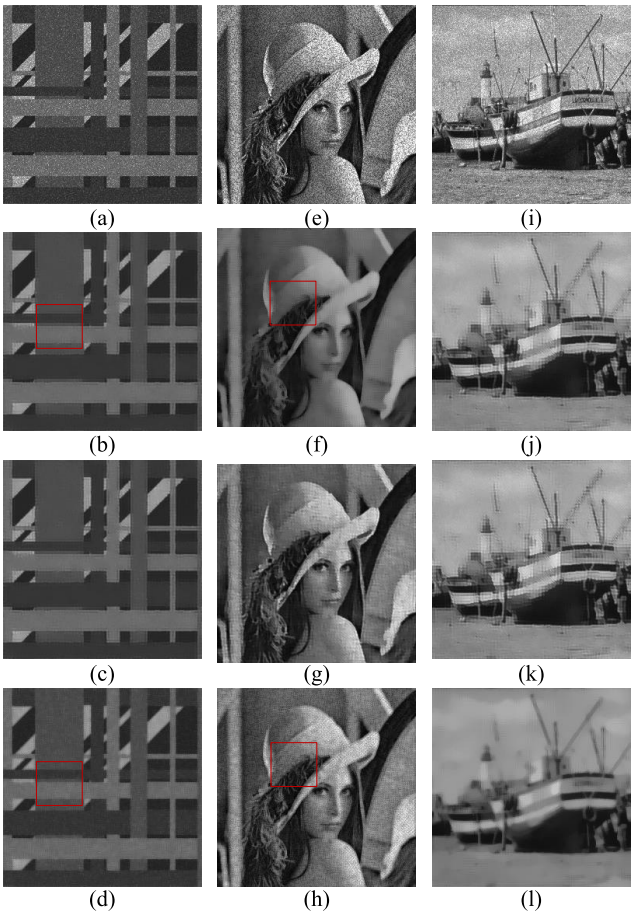

FIGURE 4. Noise removal for E01-03 experiments. (a) Gamma noisy mixedgrid image; (b) Denoised image by CSN with $\alpha = 0.5$; (c) Denoised image by CSN with $\alpha = 1$; (d) Denoised image by AA with $\alpha = 0.5$; (e) Poisson noisy Lena image; (f) Denoised image by CSN with $\alpha = 0.5$; (g) Denoised image by CSN with $\alpha = 1$; (h) Denoised image by SST with $\alpha = 0.5$; (i) Rayleigh noisy boat image; (j) Denoised image by CSN with $\alpha = 0.5$; (k) Denoised image by CSN with $\alpha = 1$; (l) Denoised image by DTDS with $\alpha = 0.5$.

In addition, the experiments were integrated into an executable application, which provides two kinds of operation modes, run with gray value animation and run with image and energy animation. The detailed information can be obtained in Appendix ''User Guidance for Supplementary Interactive application'' and ''Supplementary Interactive application''.

A. RESULTS ON SYNTHETIC MULTIPLICATIVE NOISE

First, Mixedgrid, Lena, and Boat test images with size of 256×256 were selected to evaluate the performance of our curvature-dependent variational model, the noise free image and edge features are shown in Figure 3. In E01 experiment, the Mixedgrid image was contaminated by multiplicative Gamma noise with mean 1 and variance 0.5. In E02 experiment, the Lena image was corrupted by multiplicative Poisson noise with parameter $\lambda = 2$. In E03 experiment, the boat image was corrupted by multiplicative Rayleigh noise with mean 0.8 and variance 0.08.

The visual quality of the denoising image is identified as the main evaluation standard of qualitative results. The denoising results of gamma noisy mixedgrid image (E01 experiment), Poisson noisy Lena image (E02 experiment) and Rayleigh noisy boat image (E03 experiment) are presented in Figure 4, respectively. It can be observed that the proposed method can efficiently enhance visual quality of the images, compared with the AA, SST and DTDS model.

For synthetic experiments, we calculated the common measurements of image fidelity PSNR and SSIM index [51]. The denoising results of experiment E01, E02 and E03 are depicted in Table 3. In order to investigate the robustness of the proposed method, we also carried out experiments for the parameters determination. With fixed $\beta_1, \beta_2, \beta_5 = 1$, $\frac{\beta_4}{\beta_3} = 10, \beta_3 = 15$, we tuned α from 0 to 1 with 0.1 step, the Energy, PSNR and SSIM for E01 image are strictly consistent. This also indicates that the value of α depends on the amount of noise in an image. On the other hand, with fixed $\alpha = 0.5$, parameter β_4 was assigned as 10, 50, 100, 150 and 200 to

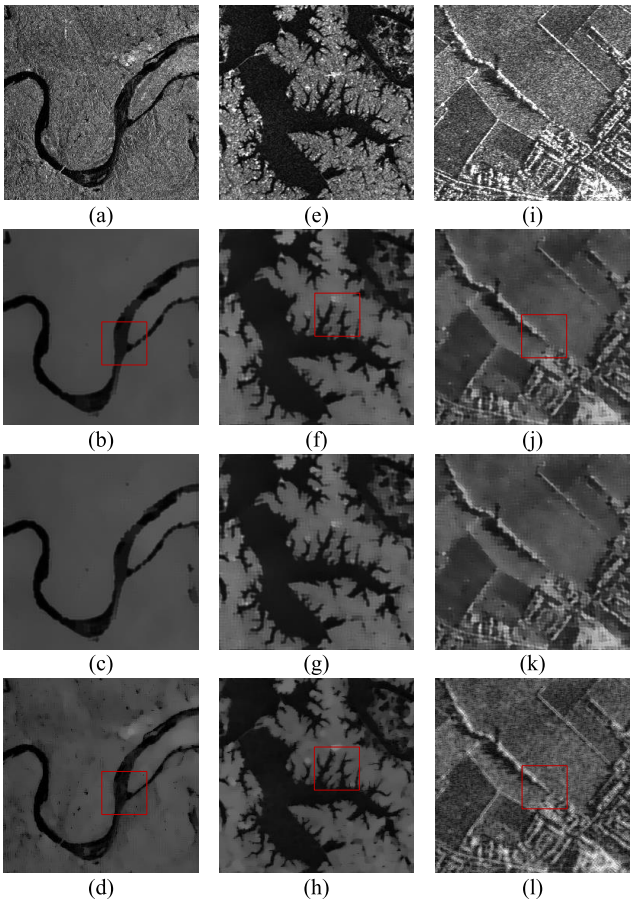

FIGURE 5. Noise removal results of SAR images. (a) SAR-1 image; (b) Denoised image by CSN with $\alpha = 0.5$; (c) Denoised image by CSN with $\alpha = 1$; (d) Denoised image by AA with $\alpha = 0.5$; (e) SAR-2 image; (f) Denoised image by CSN with $\alpha = 0.5$; (g) Denoised image by CSN with $\alpha = 1$; (h) Denoised image by AA with $\alpha = 0.5$; (i) SAR-3 image; (j) Denoised image by CSN with $\alpha = 0.5$; (k) denoised image by CSN with $\alpha = 1$; (l) Denoised image by AA with $\alpha = 0.5$.

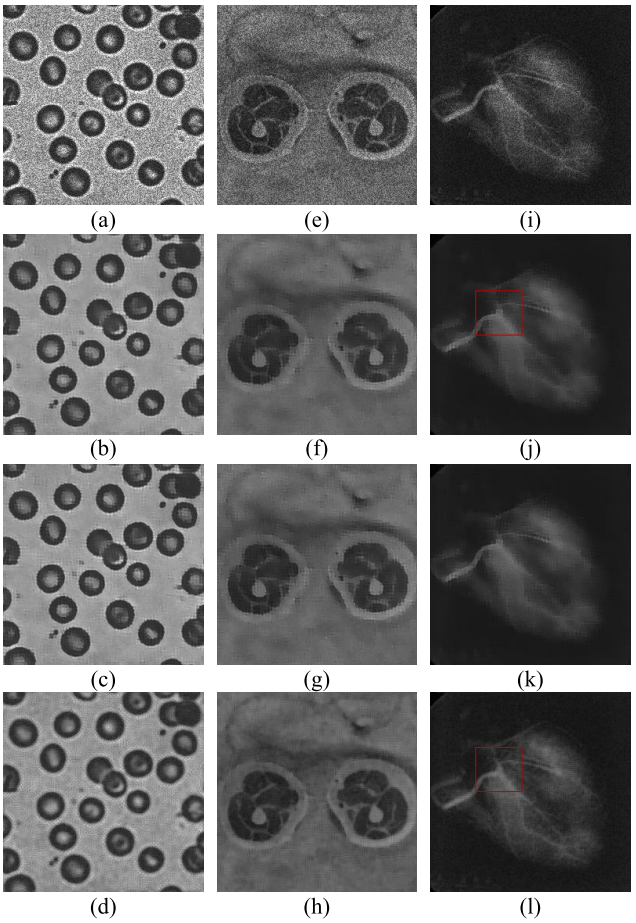

FIGURE 6. Noise removal results of Biom images. (a) Biom-1 image; (b) Denoised image by CSN with $\alpha = 0.5$; (c) Denoised image by CSN with $\alpha = 1$; (d) Denoised image by AA with $\alpha = 0.5$; (e) Biom-2 image; (f) Denoised image by CSN with $\alpha = 0.5$; (g) Denoised image by CSN with $\alpha = 1$; (h) Denoised image by AA with $\alpha = 0.5$; (i) SAR-3 image; (j) Denoised image by CSN with $\alpha = 0.5$; (k) denoised image by CSN with $\alpha = 1$; (l) Denoised image by AA with $\alpha = 0.5$.

TABLE 3. Despeckling results of experiment E01, E02 and E03.

Experiment	Noisy		Proposed variational model				Compared model	
			$\alpha = 0.5$		$\alpha = 1$		$\alpha = 0.5$	
	PSNR	SSIM	PSNR	SSIM	PSNR	SSIM	PSNR	SSIM
E01	20.58	0.4664	23.27	0.9009	23.2419	0.8951	23.68	0.7836
E02	20.32	0.4728	26.25	0.7237	28.21	0.7191	21.46	0.7325
E03	22.59	0.5805	24.68	0.6560	24.71	0.6561	22.93	0.6395

investigate the change trend of Energy, PSNR and SSIM with iterations, the results demonstrate that the smaller β_4 will accelerate the convergence, however, the denoising indicators can not perform well, with comprehensive comparison, we set $\beta_4 = 150$, $\beta_3 = 15$ for all experiments. It is worth emphasis that the PSNR for parameter $\alpha = 0.5$ and $\alpha = 1$ exists small variance. However, it is difficult to explore the intrinsic statistical law. The results illustrate that the PSNR of experiments E01 and E02 with proposed method is commonly greater than compared method. However, for experiment E01, the proposed model preserves image edges, texture better, PSNR result is not better than DTDS method.

It is well known that one certain method has different performance for different image contents, in order to carry out comprehensive comparison, experiment E04 was implemented on 500 Berkeley test images [37]. The test images were corrupted by multiplicative Gamma noise with mean 1 and variance 0.5, Poisson noise with parameter $\lambda = 2$, and Rayleigh noise with mean 0.8 and variance 0.08. To date a number of studies have been conducted on speckle noise removal and numerous despeckling filters have been proposed. Lee filter is most popular filter-based method and is a linear local statistic filter that minimizes the mean-square error for reducing speckle in images. Besides TV-based AA, SST, DTDS and so model, the denoising results were also compared with Lee filter. All the results were computed per image and then averaged over the test Berkeley dataset, as illustrated in Table 4. The results indicate that our proposed high order total curvature regularization has certain advantage compared with TV regularization and Lee filter denoising method.

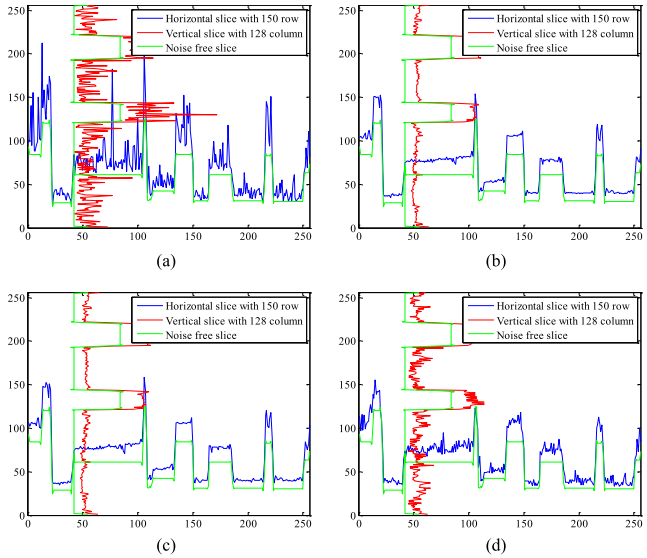

FIGURE 7. Slices plot of the noisy and denoised mixedgrid images in E01 by different models. (a) slice of noisy image; (b) slice of denoised image by proposed method with $\alpha = 0.5$; (c) slice of denoised image by proposed method with $\alpha = 1$; (d) denoised image by AA method with $\alpha = 0.5$.

B. RESULTS ON REAL SAR AND BIOMEDICAL IMAGES

The effectiveness of our proposed method were further extended to real world applications, E05 experiment was implemented to validate the efficiency of proposed method for SAR images, and E06 experiment was for biomedical images.

The SAR images of E05 experiment were assumed to follow Gamma noise distribution, the denoising results for SAR-1, SAR-2 and SAR-3 image of our method are demonstrated visually better than AA model, as shown in Figure 5.

The biomedical images of E06 experiment were assumed to follow general noise distribution, the speckle noise removal results with propose method and SO method are shown in Figure 6. It is obvious that the CSN restoration are better than SO.

TABLE 4. The average PSNR and SSIM values of 500 Berkeley test images.

Method	Gamma		Possion		Relayin	
	PSNR	SSIM	PSNR	SSIM	PSNR	SSIM
Noisy	17.3846	0.5309	12.9317	0.3384	24.0873	0.6313
Proposed	**25.2578**	**0.8367**	**23.6981**	**0.7313**	**29.6857**	**0.8942**
AA	24.3615	0.8179	-	-	-	-
SST	-	-	21.3924	0.7257	-	-
DTDS	-	-	-	-	28.6452	0.8276
SO	25.1367	0.8321	23.4632	0.6958	28.6697	0.8372
Lee filter	24.4679	0.8043	22.2457	0.7152	28.7543	0.8265

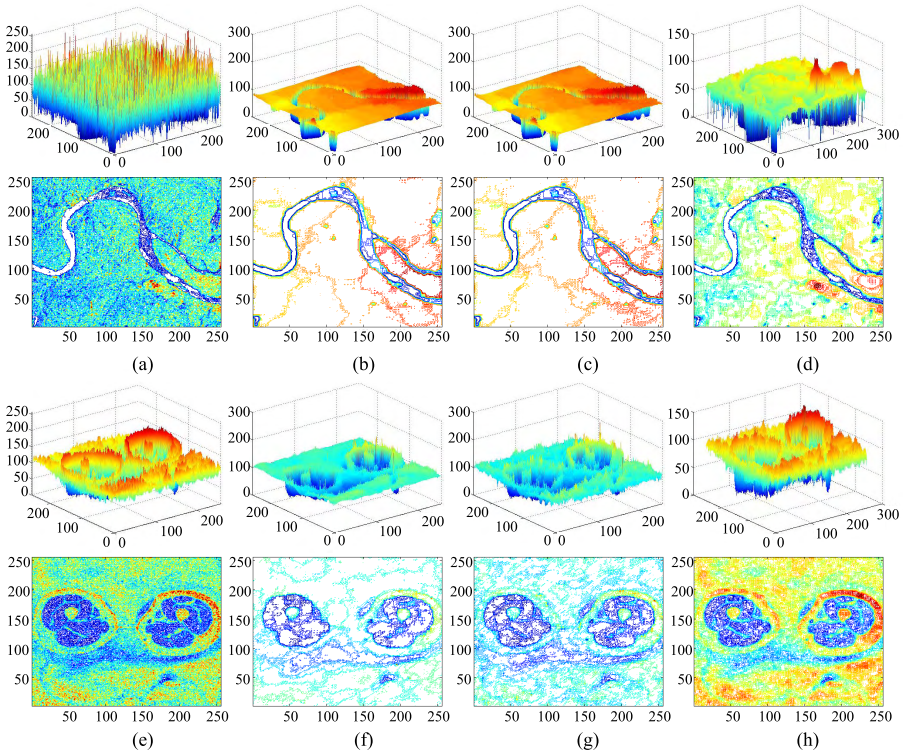

FIGURE 8. Gray value 3D and contour of the noisy and denoised images. (a) SAR-1 image; (b) Denoised SAR-1 by CSN with $\alpha = 0.5$; (c) Denoised SAR-1 by CSN with $\alpha = 1$; (d) Denoised SAR-1 by AA with $\alpha = 0.5$; (e) Biom-2 image; (f) Denoised Biom-2 by CSN with $\alpha = 0.5$; (g) Denoised Biom-2 by CSN with $\alpha = 1$; (h) Denoised Biom-2 by SO with $\alpha = 0.5$.

TABLE 5. The statistical iteration number and run time for experiments.

Exper -iment	CSN with α=0.5		CSN with α=1		Compared method	
	Iteration number	Run time(s)	Iteration number	Run time(s)	Iteration number	Run time(s)
E01	62	6.65	62	6.65	138	8.11
E02	34	4.10	34	4.07	696	45.49
E03	63	7.94	63	8.26	528	34.04
E05-1	173	16.94	172	16.98	1205	62.73
E05-2	38	3.92	38	13.93	1029	57.06
E05-3	30	3.17	36	3.71	7	0.52
E06-1	65	7.11	65	7.01	172	9.98
E06-2	65	6.81	65	7.16	367	20.63
E06-3	64	7.13	64	6.86	133	7.47

C. EDGE PRESERVING AND STAIRCASE EFFECT ANALYSIS

Slices of original, noisy and restoration mixedgrid image in E01 experiment are illustrated in Figure 7. The denoising horizontal (blue) and vertical slice curve (red) can overlap with original slice curve (green) almost, consequently, the proposed model can preserve the edge and corner of image. Further, it can be observed that the slice curve of restoration image slightly deviates from original one, the main reason is the loss of image contrast.

Spatial and temporal variance for gray value of SAR-1 image in E05 and Biom-2 image in E06 are also used to demonstrate the edge preserve performance of different methods, which are presented in Figure 8. The three dimensional (3D) and contour of SAR-1 and Biom-2 image illustrate that proposed method can improve image features, meanwhile, the edges and corners are well preserved.

As well known, the first-order TV model leads to staircase effect, that is, the restored image appears jagged. For a local region comparison, we amplified regions indicated by the red rectangles in Figure 4, 5,and 6 to Figure 9 from which we can see the performance of each model more clearly. It can be easily judged that the proposed model provides more natural effect with clearer details. As is seen from the results, AA and SST reduce the noise but blurring the images. DTDS model shows better performance with a little noise remained. Furthermore, AA, SST and DTDS model generate different degree of staircase effect in the flat region which can be easily observed in Lena's hat. It is clearly seen that the proposed model reduces the staircase effect and preserve the edges, textures and fine details which can be easily seen in the geometric edge of Mixedgrid image and the hair of Lena image.

D. CONVERGENCE ANALYSIS

For iteration stopping criteria Eq.(44) with $threshold = 10^{-3}$, the computational time is measured in seconds and iteration number are illustrated in Table 5. Compared with AA, SST, DTDS and SO model under split Bregman algorithm,

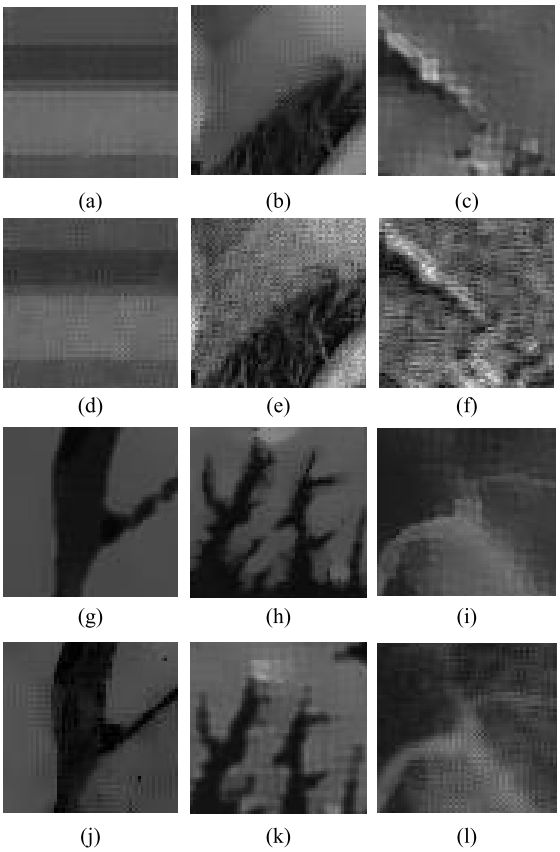

FIGURE 9. Zoom in small sub-regions of images in Figure 4,5 and 6 for detail comparison; (a) Denoised image of E01 CSN; (b) Denoised image of E02 CSN; (c) Denoised image of E05-3 CSN; (d) Denoised image of E01 AA; (e) Denoised image of E02 SST; (f) Denoised image of E05-3 DTDS CSN; (g) Denoised image of E05-1 CSN; (h) Denoised image of E05-2 CSN; (i) Denoised image of E06-3 CSN; (j) Denoised image of E05-1 AA; (k) Denoised image of E05-2 SST; (l) Denoised image of E06-3 DTDS.

the run speed of proposed method can be identified faster except E05-3, furthermore, our algorithm takes less iteration to converge.

During the iterations, the numerical energy E^k, residuals $R_1^k, R_2^k, \vec{R}_3^k, R_4^k, \vec{R}_5^k$ defined by Eq.(45), relative error in u^k defined by Eq.(46), PSNR and SSIM were always monitored, which will give us important information about the convergence of the iterations.

$$\begin{aligned} R_1^k &= \int_\Omega \left(z^k - w^k\right) \\ R_2^k &= \int_\Omega \left(\left|\vec{p}^k\right| - \vec{m}^k \cdot \vec{p}^k\right) \\ \vec{R}_3^k &= \int_\Omega \left(\vec{p}^k - \nabla u^k\right) \\ R_4^k &= \int_\Omega \left(q^k - \nabla \cdot \vec{n}^k\right) \\ \vec{R}_5^k &= \int_\Omega \left(\vec{n}^k - \vec{m}^k\right) \end{aligned} \tag{45}$$

$$relativeerror = \frac{\int_\Omega \left(u^k - u^{k-1}\right)}{\int_\Omega u^k} \tag{46}$$

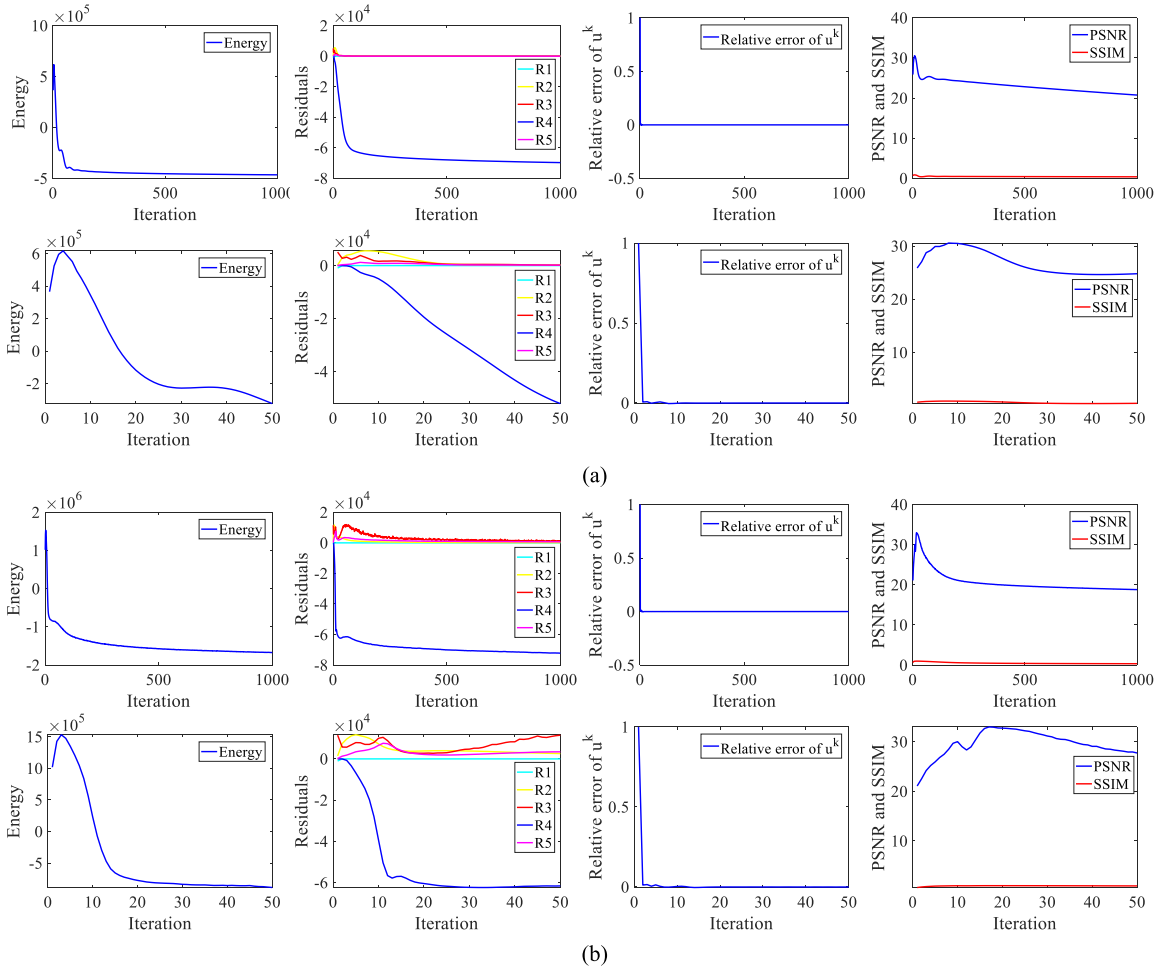

FIGURE 10. Convergence analysis. (a) From left, first and second rows are plots of residuals $R_1^k, R_2^k, \tilde{R}_3^k, R_4^k, \tilde{R}_5^k$, relative error in u^k, energy E^k, PSNR and SSIM for E01 experiment of 1000 iterations and 50 iterations, respectively;(b) From left, third and fourth rows are plots of residuals $R_1^k, R_2^k, \tilde{R}_3^k, R_4^k, \tilde{R}_5^k$, relative error in u^k, energy E^k, PSNR and SSIM for E21 experiment of 1000 iterations and 50 iterations, respectively.

$(\cdot)^k$ denotes the variable value of current k iteration. Since the nonlinearity, nonconvexity of proposed model, the energy convergence was analyzed deeply, all quantities are plotted up to 1000 iterations, and furthermore, the earlier 50 iterations are amplified into the following rows, as shown in Figure 10. The graphs on the first and second rows, third and fourth rows are related to the E01, E02 experiments respectively. The plots of the other experiments also have similar profiles in Figure 10. Due to energy functional is not convex, we should not expect strict monotonic decreasing in the residuals, the relative error, the energy. However, the algorithm is stable and has converged, it is also clear that PSNR and SSIM have converged to a steady state. And it is important that the relative error in u^k converged to zero at high speed. It is need to clarify that the increasing and short-term oscillation profile of energy in early stage of iteration is reasonable, because variables $\vec{p}$, q, $\vec{n}$, $\vec{m}$, λ_1, λ_2, $\vec{\lambda}_3$, λ_4, $\vec{\lambda}_5$ are initialized as zero. Starting with zero values, the fidelity term of Eq.(16) tends to zero and regularity term of Eq.(16) is increasing, eventually, the numerical energy is steady and downward after a few iterations.

VI. CONCLUSIONS

A novel high order variational model and its fast algorithm for speckle noise removal were proposed in this paper. The most relevant conclusions are summarized as follows:

(1) A high order variational model for image restoration based on total curvature was proposed, the model can remove multiplicative noise as well as preserving image features.

(2) The proposed model has nonlinearity, nonconvexity and high order derivative. Due to these features, a series of constraints were specially designed with penalization techniques.

(3) A fast comprehensive alternating minimization iteration scheme, which is based on FFT, gradient descend, soft thresholding formula and projection method, were constructed to solve PDE derived from minimization of optimization problem with constraints.

(4) Experimental results reveal that the new model can improve visual quality in term of PSNR, SSIM and preserve edge and corner features of the restored image better than other variational model.

(5) Meanwhile, numerical results indicate the fast algorithm can generate good results in terms of convergence speed and computational time as well.

Although the proposed model is mainly based on the total curvature regularization, within this higher-order curvature convex variation modeling framework, there are various potential to obtain better outlook.

(1) The regularization term can be extended to other high order regularization, such as Laplacian, Hessian, Fourth-order derivative.

(2) Impulsive noise is very common in data acquisition and transmission [52], and TV is an popular prior model for impulse noise remove [53]. Due to the speckle noise has always been accompanied by impulse noise, the proposed high-order modeling method can be generalized to surpress simultaneously speckle and impulsive noise.

(3) Even if TV has staircase effect, it outperforms many image restoration methods and has a high performance to preserve image edge. So TV and high-order combination, such as $\left(a + b\left(\nabla \cdot \frac{\nabla u}{|\nabla u|}\right)\right)(c + d\,|\nabla u|)$, will be an effective and prior model in the field of regularization based image processing.

(4) Algorithmically, the Lagrange multipliers and variables are initialized to zero for simplicity, it is possible to obtain faster numerical results by changing the initialization.

Consequently, the further research can expose some interesting issues about the high order variational model for speckle noise removal and other image processing problems.

REFERENCES

[1] S. Durand, J. Fadili, and M. Nikolova, "Multiplicative noise cleaning via a variational method involving curvelet coefficients," in *Proc. Int. Conf. Scale Space Variational Methods Comput. Vis.*, Jun. 2009, pp. 282–294.

[2] K. Krissian, C.-F. Westin, R. Kikinis, and K. G. Vosburgh, "Oriented speckle reducing anisotropic diffusion," *IEEE Trans. Image Process.*, vol. 16, no. 5, pp. 1412–1424, May 2007.

[3] Y.-M. Huang, M. K. Ng, and Y.-W. Wen, "A new total variation method for multiplicative noise removal," *SIAM J. Imag. Sci.*, vol. 2, no. 1, pp. 20–40, 2009.

[4] S. Durand, J. Fadili, and M. Nikolova, "Multiplicative noise removal using L1 fidelity on frame coefficients," *J. Math. Imag. Vis.*, vol. 36, no. 3, pp. 201–226, 2010.

[5] Y. Dong and T. Zeng, "A convex variational model for restoring blurred images with multiplicative noise," *SIAM J. Imag. Sci.*, vol. 6, no. 3, pp. 1598–1625, 2013.

[6] J. Dong, Z. Han, Y. Zhao, W. Wang, A. Prochazka, and J. Chambers, "Sparse analysis model based multiplicative noise removal with enhanced regularization," *Signal Process.*, vol. 137, pp. 160–176, Aug. 2017.

[7] A. Ullah, W. Chen, H. Sun, and M. A. Khan, "A modified multi-grid algorithm for a novel variational model to remove multiplicative noise," *J. Vis. Commun. Image Represent.*, vol. 40, pp. 485–501, Oct. 2016.

[8] M. Hacini, F. Hachouf, and K. Djemal, "A new speckle filtering method for ultrasound images based on a weighted multiplicative total variation," *Signal Process.*, vol. 103, pp. 214–229, Oct. 2014.

[9] J. Zhang, G. Lin, L. Wu, and Y. Cheng, "Speckle filtering of medical ultrasonic images using wavelet and guided filter," *Ultrasonics*, vol. 65, pp. 177–193, Feb. 2016.

[10] L. L. Yao, X. C. Feng, and Y. F. Li, "Principal component analysis method for muitiplicative noise removal," *Acta Photonica Sinica*, vol. 40, no. 7, pp. 1031–1035, 2011.

[11] V. P. Romero, L. Maffei, G. Brambilla, and G. Ciaburro, "Modelling the soundscape quality of urban waterfronts by artificial neural networks," *Appl. Acoust.*, vol. 111, pp. 121–128, Oct. 2016.

[12] W. Lu, J. Duan, Z. Qiu, Z. Pan, R. W. Liu, and L. Bai, "Implementation of high-order variational models made easy for image processing," *Math. Methods Appl. Sci.*, vol. 39, no. 14, pp. 4208–4233, 2016.

[13] B. Shi, L. Huang, and Z.-F. Pang, "Fast algorithm for multiplicative noise removal," *J. Vis. Commun. Image Represent.*, vol. 23, no. 1, pp. 126–133, 2012.

[14] T. Lv, X. Han, S. Wu, and Y. Li, "The effect of speckles noise on the Laser Doppler Vibrometry for remote speech detection," *Opt. Commun.*, vol. 440, pp. 117–125, Jun. 2019.

[15] R. Sivaranjani, S. M. M. Roomi, and M. Senthilarasi, "Speckle noise removal in SAR images using Multi-Objective PSO (MOPSO) algorithm." *Appl. Soft Comput.*, vol. 76, pp. 671–681, Mar. 2019.

[16] P. Mangalraj and A. Agrawal, "Despeckling of SAR images by directional representation and directional restoration," *Optik*, vol. 127, no. 1, pp. 116–121, 2016.

[17] C. Zou and Y. Xia, "Bayesian dictionary learning for hyperspectral image super resolution in mixed Poisson–Gaussian noise," *Signal Process., Image Commun.*, vol. 60, pp. 29–41, Feb. 2018.

[18] A. Khvostikov, A. Krylov, J. Kamalov, and A. Megroyan, "Ultrasound despeckling by anisotropic diffusion and total variation methods for liver fibrosis diagnostics," *Signal Process., Image Commun.*, vol. 59, pp. 3–11, Nov. 2017.

[19] L. Rudin, P. L. Lions, and S. Osher, *Multiplicative Denoising Deblurring: Theory Algorithms*. New York, NY, USA: Springer, 2003.

[20] G. Aubert and J.-F. Aujol, "A variational approach to removing multiplicative noise," *SIAM J. Appl. Math.*, vol. 68, no. 4, pp. 925–946, 2008.

[21] J. Shi and S. Osher, "A nonlinear inverse scale space method for a convex multiplicative noise model," *SIAM J. Imag. Sci.*, vol. 1, no. 3, pp. 294–321, 2008.

[22] H. Zhang, L. Tang, Z. Fang, C. Xiang, and C. Li, "Nonconvex and nonsmooth total generalized variation model for image restoration," *Signal Process.*, vol. 143, pp. 69–85, Feb. 2018.

[23] L. Denis, F. Tupin, J. Darbon, and M. Sigelle, "Sar image regularization with fast approximate discrete minimization," *IEEE Trans. Image Process.*, vol. 18, no. 7, pp. 1588–1600, Jul. 2009.

[24] S. Setzer, G. Steidl, and T. Teuber, "Deblurring Poissonian images by split Bregman techniques," *J. Vis. Commun. Image Represent.*, vol. 21, no. 3, pp. 193–199, Apr. 2010.

[25] Z. Jin and X. Yang, "Analysis of a new variational model for multiplicative noise removal," *J. Math. Anal. Appl.*, vol. 362, no. 2, pp. 415–426, 2010.

[26] M.-G. Shama, T.-Z. Huang, J. Liu, and S. Wang, "A convex total generalized variation regularized model for multiplicative noise and blur removal," *Appl. Math. Comput.*, vol. 276, pp. 109–121, Mar. 2016.

[27] S. Li, G. Wang, and X. Zhao, "Multiplicative noise removal via adaptive learned dictionaries and TV regularization," *Digit. Signal Process.*, vol. 50, pp. 218–228, Mar. 2016.

[28] P. Singh and R. Shree, "A new SAR image despeckling using directional smoothing filter and method noise thresholding," *Eng. Sci. Technol., Int. J.*, vol. 21, no. 4, pp. 589–610, 2018.

[29] F. Li, C. Shen, J. Fan, and C. Shen, "Image restoration combining a total variational filter and a fourth-order filter," *J. Vis. Commun. Image Represent.*, vol. 18, no. 4, pp. 322–330, 2007.

[30] M. R. Hajiaboli, "A self-governing fourth-order nonlinear diffusion filter for image noise removal," *IPSJ Trans. Comput. Vis. Appl.*, vol. 2, pp. 94–103, May 2010.

[31] Y. Hao, J. Xu, S. Li, and X. Zhang, "A variational model based on split Bregman method for multiplicative noise removal," *AEU-Int. J. Electron. Commun.*, vol. 69, no. 9, pp. 1291–1296, 2015.

[32] W. Hinterberger and O. Scherzer, "Variational methods on the space of functions of bounded hessian for convexification and denoising," *Computing*, vol. 76, nos. 1–2, pp. 109–133, 2006.

[33] J. Duan, Z. Qiu, W. Lu, G. Wang, Z. Pan, and L. Bai, "An edge-weighted second order variational model for image decomposition," *Digit. Signal Process.*, vol. 49, pp. 162–181, Feb. 2016.

[34] J. Duan, W. O. C. Ward, L. Sibbett, Z. Pan, and L. Bai, "Introducing diffusion tensor to high order variational model for image reconstruction," *Digit. Signal Process.*, vol. 69, pp. 323–336, Oct. 2017.

[35] B. Goldluecke and D. Cremers, "Introducing total curvature for image processing," in *Proc. Int. Conf. Comput. Vis.*, Nov. 2011, pp. 1267–1274.
[36] X. C. Tai, "Fast numerical schemes related to curvature minimization: A brief and elementary review," *Actes des Rencontres du CIRM*, vol. 3, no. 1, pp. 17–30, 2013.
[37] Y. Chen, W. Feng, R. Ranftl, H. Qiao, and T. Pock, "A higher-order MRF based variational model for multiplicative noise reduction," *IEEE Signal Process. Lett.*, vol. 21, no. 11, pp. 1370–1374, Nov. 2014.
[38] A. Chambolle, "An algorithm for total variation minimization and applications," *J. Math. Imag. Vis.*, vol. 20, no. 1, pp. 89–97, 2004.
[39] T. F. Chan, G. H. Golub, and P. Mulet, "A nonlinear primal-dual method for total variation-based image restoration," *SIAM J. Sci. Comput.*, vol. 20, no. 6, pp. 1964–1977, 1999.
[40] E. Ernie, "Applications of Lagrangian-based alternating direction methods and connections to split Bregman," CAM Rep. 9, 2009.
[41] E. Esser, X. Zhang, and T. Chan, "A general framework for a class of first order primal-dual algorithms for TV minimization," Ucla Cam Rep., 2009, pp. 9–67.
[42] P. Weiss and L. Blanc-Féraud, and G. Aubert, "Efficient schemes for total variation minimization under constraints in image processing," *SIAM J. Sci. Comput.*, vol. 31, no. 3, pp. 2047–2080, 2009.
[43] C. Wu and X.-C. Tai, "Augmented Lagrangian method, dual methods, and split Bregman iteration for ROF, vectorial TV, and high order models," *SIAM J. Imag. Sci.*, vol. 3, no. 3, pp. 300–339, Jan. 2010.
[44] T. F. Chan and P. Mulet, "On the convergence of the lagged diffusivity fixed point method in total variation image restoration," *SIAM J. Numer. Anal.*, vol. 36, no. 2, pp. 354–367, 1999.
[45] G. Steidl and T. Teuber, "Removing multiplicative noise by Douglas-Rachford splitting methods," *J. Math. Imag. Vis.*, vol. 36, no. 2, pp. 168–184, 2010.
[46] D.-Q. Chen, X.-P. Du, and Y. Zhou, "Primal–dual algorithm based on Gauss–Seidel scheme with application to multiplicative noise removal," *J. Comput. Appl. Math.*, vol. 292, pp. 609–622, Jan. 2016.
[47] Y. Hao and J. Xu, "An effective dual method for multiplicative noise removal," *J. Vis. Commun. Image Represent.*, vol. 25, no. 2, pp. 306–312, 2014.
[48] P. Getreuer, "Rudin-osher-fatemi total variation Denoising using split Bregman," *Image Process. Line*, vol. 2, pp. 74–95, May 2012.
[49] L. Huang, L. Xiao, and Z. Wei, "A nonlinear inverse scale space method for multiplicative noise removal based on Weberized total variation," in *Proc. 5th Int. Conf. Image Graph.*, 2009, pp. 119–123.
[50] X. C. Tai, J. Hahn, and G. J. Chung, "A fast algorithm for Euler's elastica model using Augmented Lagrangian method," *SIAM J. Imag. Sci.*, vol. 4, no. 1, pp. 313–344, 2011.
[51] Z. Wang, A. C. Bovik, H. R. Sheikh, and E. P. Simoncelli, "Image quality assessment: From error visibility to structural similarity," *IEEE Trans. Image Process.*, vol. 13, no. 4, pp. 600–612, Apr. 2004.
[52] J.-L. Yin, B.-H. Chen, and Y. Li, "Highly accurate image reconstruction for multimodal noise suppression using semisupervised learning on big data," *IEEE Trans. Multimedia*, vol. 20, no. 11, pp. 3045–3056, Nov. 2018.
[53] C. L. P. Chen, L. Licheng, C. Long, T. Y. Yan, and Z. Yicong, "Weighted couple sparse representation with classified regularization for impulse noise removal," *IEEE Trans. Image Process. A Publication IEEE Signal Process. Soc.*, vol. 24, no. 11, pp. 4014–4026, Nov. 2015.

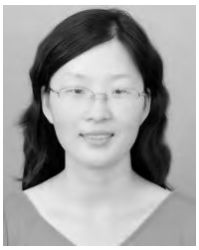

BAOXIANG HUANG received the M.S. degree in mechatronic engineering from Shandong University, China, in 2005, and the Ph.D. degree in computer engineering from the Ocean University of China, China. She is currently an Associate Professor with the College of Computer Science and Technology, Qingdao University, Qingdao, China, and is also an academic visitor of the University of Nottingham, U.K. Her research interests include remote sensing image processing and analysis, urban acoustic environment modeling, and quality assessment.

YUNPING MU received the B.S. degree in the Internet of Things engineering from Qingdao University, China, in 2017, where she is currently pursuing the M.S. degree. Her research interests include image deniosing and segmentation.

ZHENKUAN PAN received the B.E. degree from Northwestern Polytechnical University, Xi'an, China, in 1987, and the Ph.D. degree from Shanghai Jiao Tong University, Shanghai, China, in 1992. He is currently a Professor with the College of Computer Science and Technology, Qingdao University, Qingdao, China. He has authored or coauthored over 300 academic papers in the areas of computer vision, dynamics, and control. His research interest includes variational models of image and geometry processing and multibody system dynamics.

LI BAI received the B.Sc. and M.Sc. degrees in mathematics from China, and the Ph.D. degree in computer science from the University of Nottingham. She is currently with the School of Computer Science, University of Nottingham. She is interested in the use of mathematics, machine learning, and AI techniques for research in computer vision, pattern recognition, and medical imaging applications. She has published over 200 refereed papers in journals and conferences.

HUAN YANG received the B.S. degree in computer science from the Heilongjiang Institute of Technology, China, in 2007, the M.S. degree in computer science from Shandong University, China, in 2010, and the Ph.D. degree in computer engineering from Nanyang Technological University, Singapore, in 2015. She is currently a Lecturer with the College of Computer Science and Technology, Qingdao University, Qingdao, China. Her research interests include image/video processing and analysis, perception-based modeling and quality assessment, object detection/recognition, and machine learning.

JINGMING DUAN received the Ph.D. degree in computer science from the University of Nottingham, U.K. From 2017 to 2019, he was a Research Associate with the Imperial College London, U.K. He is currently a Lecturer with the University of Birmingham, U.K. His research interests include deep neural networks, variational methods, partial/ordinary differential equations, numerical optimization, and finite difference/element methods, with applications to image processing, computer vision, and medical imaging analysis.